Geophysical Research Letters

RESEARCH LETTER
10.1029/2023GL104977

Key Points:

- Space-based observations and reanalysis are considered to determine the factors that control how mixed mixed-phase clouds are
- Liquid dominated clouds contain small and isolated ice pockets whereas ice dominated clouds contain large and isolated liquid pockets
- Temperature and black carbon play an important role in controlling the cloud phase spatial distribution and increasing phase heterogeneity

Supporting Information:

Supporting Information may be found in the online version of this article.

Correspondence to:

Q. Coopman,
quentin.coopman@mcgill.ca

Citation:

Coopman, Q., & Tan, I. (2023). Characterization of the spatial distribution of the thermodynamic phase within mixed-phase clouds using satellite observations. *Geophysical Research Letters*, *50*, e2023GL104977. https://doi.org/10.1029/2023GL104977

Received 14 DEC 2022
Accepted 17 SEP 2023

Author Contributions:

Conceptualization: Q. Coopman, I. Tan
Funding acquisition: I. Tan
Investigation: Q. Coopman, I. Tan
Methodology: Q. Coopman, I. Tan
Supervision: I. Tan
Validation: Q. Coopman
Visualization: Q. Coopman
Writing – original draft: Q. Coopman
Writing – review & editing: Q. Coopman, I. Tan

Characterization of the Spatial Distribution of the Thermodynamic Phase Within Mixed-Phase Clouds Using Satellite Observations

Q. Coopman[1] **and I. Tan**[1]

[1]Department of Atmospheric and Oceanic Sciences, McGill University, Montreal, QC, Canada

Abstract Models assume that mixed-phase clouds consist of uniformly mixed ice crystals and liquid cloud droplets when observations have shown that they consist of clusters, or "pockets," of ice crystals and liquid cloud droplets. We characterize the spatial distribution of cloud phase over the Arctic and the Southern Ocean using active satellite observations and determine the relative importance of collocated meteorological parameters and aerosols from reanalysis to predict how uniformly mixed mixed-phase clouds are for the first time. We performed a multi-linear regression fit to the data set to predict the spatial distribution of the ice and liquid pockets. Contrary to what models suggest, mixed-phase clouds are rarely perfectly homogeneous. Our results suggest that high temperatures are associated with homogeneously mixed ice and liquid pockets. We also find that a high mixing ratio of black carbon is associated with heterogeneously mixed ice and liquid pockets.

Plain Language Summary The representation of clouds in numerical models remains one of the largest uncertainties in predicting our future climate. Clouds can consist solely of liquid droplets, ice crystals, or the coexistence of both hydrometeor types. The latter cloud type is referred to as mixed phase. Climate models assume that liquid droplets and ice crystals are uniformly mixed in space in mixed-phase clouds, but observations show that mixed-phase clouds are organized in separate pockets of clustered liquid droplets and ice crystals. This difference in representation has a large impact on the lifetime of clouds and on their role in climate change. Using satellite observations over the Arctic and the Southern Ocean, we quantify the spatial distribution of ice and liquid in clouds. We used a statistical method to determine the relationship between meteorology and aerosols and the spatial distribution of ice and liquid. Our results suggest that high temperatures are associated with homogeneously mixed mixed-phase clouds and high concentrations of soot are associated with heterogeneously mixed mixed-phase clouds. Furthermore, pockets of liquid within ice clouds are larger than pockets of ice within liquid clouds. These results will improve the representation of mixed-phase clouds in large-scale models.

1. Introduction

Clouds continue to be poorly represented in Global Climate Models (GCMs) (Vignesh et al., 2020). One particular cloud type that GCMs continue to struggle to represent are mixed-phase clouds that exist at temperatures between −38 and 0°C which are particularly ubiquitous in the Arctic and Southern Ocean (Coopman et al., 2021; Korolev et al., 2017; Listowski et al., 2019; Matus & L'Ecuyer, 2017; Mioche et al., 2015; Nomokonova et al., 2019; Shupe, 2011; Shupe et al., 2006; Wang et al., 2003; Zhao & Wang, 2010). Large-scale forcing, dynamics, surface conditions, and microphysical, radiative, and turbulent processes all contribute to the life cycle of mixed-phase clouds (Morrison et al., 2011). These microphysical processes include aerosol particle activation, secondary ice processes, heterogeneous nucleation (Kalesse et al., 2016; Solomon et al., 2018), and also the Wegener-Bergeron-Findeisen (WBF) process, which was shown to be among largest contributors to the partitioning of liquid and ice in mixed-phase clouds in a GCM (Tan et al., 2016). The WBF process describes the growth of ice crystals at the expense of nearby liquid cloud droplets in mixed-phase clouds (Bergeron, 1935; Findeisen, 1938; Wegener, 1911) when the in-cloud vapor pressure is between the saturation vapor pressure over liquid water and the lower saturation vapor pressure over ice (Korolev, 2007). The WBF process is thus more efficient when hydrometeors are uniformly mixed than when organized in discrete pockets of ice crystals and liquid droplets. Independent aircraft in situ as well as ground-based and satellite remote sensing observations support the latter arrangement of cloud thermodynamic phase, that is, hydrometeors tend to be organized in pockets or clusters of ice crystals and liquid droplets (Chylek & Borel, 2004; D'Alessandro et al., 2019;

Korolev & Milbrandt, 2022; Korolev et al., 2003; Lewis et al., 2020; Shupe, 2007; Thompson et al., 2018). Nonetheless, GCMs assume that cloud droplets and ice crystals within mixed-phase clouds are uniformly mixed (e.g., Gettelman et al., 2010). This implies that GCMs glaciate mixed-phase clouds too efficiently compared to what is observed in nature (Cesana et al., 2015; Komurcu et al., 2014). Although the tendency of mixed-phase clouds to glaciate too efficiently has recently been reduced in some GCMs (Bodas-Salcedo et al., 2019; Zelinka et al., 2020; Y. Zhang et al., 2019), biases have been overcompensated in some cases (M. Zhang et al., 2019), and all GCMs thus far have achieved this by applying an arbitrary tuning factor.

GCMs ultimately need to account for the heterogeneity of the cloud thermodynamic phase distribution to represent more realistically mixed-phase clouds. This can in turn aid in maintaining the proportion of supercooled liquid water in mixed-phase clouds and has ramifications for both how accurately the cloud radiative effect is represented and how it will change as our climate evolves. The latter effect is related to future climate projections. In particular, the surface temperature-mediated response of clouds—known as the cloud feedback—remains the largest contributor to uncertainty in climate radiative feedbacks (Forster et al., 2021). The cloud-phase feedback (Mitchell et al., 1989) in particular, pertains to the shift in cloud thermodynamic phase from ice to liquid in response to global warming. As liquid clouds are more reflective than ice clouds for the same water content (Pruppacher & Klett, 2010), the cloud-phase feedback is negative. Increasing the proportion of supercooled liquid in mixed-phase clouds in GCMs has been shown to increase global climate sensitivity via the cloud-phase feedback (Frey & Kay, 2018; Tan et al., 2016).

Several methods have been developed to describe the cloud phase distribution within mixed-phase clouds (Coopman et al., 2021). However, their method did not consider the liquid-ice interface, and thus, no conclusion could be drawn regarding the efficiency of the WBF process.

The first step in improving GCM subgrid-scale variability in cloud phase is, on the one hand, to characterize the spatial distribution of ice and liquid pixels within mixed-phase clouds using observations and, on the other hand, to determine what conditions control it. Active satellite observations are suitable for this purpose, as they provide nearly global coverage of the vertical structure of the cloud phase with a vertical resolution of approximately 60 m and with a horizontal spatial resolution of up to a few hundred meters over a long period of time. Active instruments have a better representation of the cloud fraction (Chan & Comiso, 2013) and the cloud thermodynamic phase (Peterson et al., 2020) compare to passive instruments. Nevertheless, it should be noted that active measurements from space-based instruments have more uncertainties compared to in situ and ground-based observations (Tansey et al., 2022) (e.g., inability to observe small particles, low-level clouds near the ground, and all multilayer clouds, the coarse spatial resolution, algorithm errors due to incorrect simplifying assumptions) and the data set might not be able to accurately quantify cloud base due to signal attenuation. Recent studies have quantified the heterogeneity of mixed-phase clouds over the mid-latitude and Arctic regions (D'Alessandro et al., 2019; Korolev & Milbrandt, 2022). However, studies investigating the control of the global spatial distribution of the thermodynamic and local meteorological parameters on phase heterogeneity are scarce.

To this end, we employ active satellite observations to define a metric that quantifies the spatial distribution of liquid and ice pixels within mixed-phase clouds. We collocate the metric with reanalysis and determine the most important parameters from a multilinear regression model.

2. Data Set

We use DARDAR-MASK (raDAR/liDAR) v.2 (Ceccaldi et al., 2013; Delanoë & Hogan, 2008, 2010), which retrieves the vertical profile of cloud properties with the synergy of CloudSat Cloud Profiling Radar (Stephens et al., 2002) and the Cloud-Aerosol Lidar and Infrared Pathfinder Satellite Observation (CALIPSO) lidar, Cloud-Aerosol Lidar with Orthogonal Polarization (CALIOP) (Winker et al., 2007, 2009), both of which are space-based instruments that are part of the A-train constellation. DARDAR has a footprint resolution of 1.4 km and a vertical resolution of 60 m between the surface and 25.08 km and has shown satisfactory results to classify clouds (Ceccaldi et al., 2013; Listowski et al., 2019, 2020) (see Text S1 in Supporting Information S1 for details). Nevertheless, Hagihara and Okamoto (2013) have shown that aerosols can be misclassified as clouds by the CALIPSO algorithm, potentially biasing the present analysis. It is important to note that there is not a common definition for mixed-phase clouds, and it depends on the spatial resolution of interest (Korolev et al., 2017). For example, whereas a satellite pixel resolution is on the order of 1 km, in situ measurements can observe individual

hydrometeors, depending on the speed of the aircraft, and thus identify a cloud composed mainly of liquid droplets with only one ice crystal as mixed phase that a satellite instrument would otherwise not be capable of identifying due to limitations pertaining to spatial resolution. We also discarded pixels categorized as precipitating ice (ice pixels that are connected to the surface) because although they may be considered to be part of the cloud, we assume that existing below the cloud they do not impact the WBF process.

It is important to note that the use of DARDAR may underestimate the number of mixed-phase clouds relative to in situ observations that have observed smaller pockets of liquid and ice clouds (D'Alessandro et al., 2019; Korolev & Milbrandt, 2022) since the minimum pocket size is limited by the resolution of the instrument. Using observations compatible with satellite simulators such as Cloud Feedback Model Intercomparison Project (CFMIP) Observation Simulator Package (COSP) (Cesana & Chepfer, 2013) could help compensate instrument limitations but would still impact model parametrizations since they are cloud-top biased. We did not consider pixels lower than 1 km in altitude to avoid limitations of the radar related to ground clutter. It should be noted that CloudSat might miss some small ice crystals but they can be detected by CALIOP (Avery et al., 2012). The present study focuses on the vertical spatial distribution of the cloud thermodynamic phase using retrievals from DARDAR, but we did not investigate the distribution across the satellite orbit track.

We collocated the cloud-level temperature, vertical velocity, surface latent heat flux, surface sensible heat flux, specific humidity, and the temperature profile of the atmosphere. These meteorological parameters are obtained from the European Centre for Medium-Range Weather Forecasts (ECMWF) ReAnalysis fifth generation (ERA5) (Hersbach et al., 2020). The data set is based on a $0.25° \times 0.25°$ grid with a vertical resolution between 25 and 50 hPa representing the large scale and with a temporal resolution of 3 hr showing satisfactory results when compared to observations (Graham et al., 2019). We also considered the lower tropospheric stability (LTS) from ERA-5, to represent the stability of the lower atmosphere which has been shown to strongly impact low-cloud properties (Kay & Gettelman, 2009; Klein & Hartmann, 1993) (see Text S2 in Supporting Information S1 for details).

We also collocated the cloud thermodynamic phase information with the aerosol mixing ratio from Modern-Era Retrospective analysis for Research and Applications, version 2 (MERRA-2) reanalysis (Gelaro et al., 2017). MERRA-2 retrieves aerosols properties with a spatial resolution of 0.5° in latitude, 0.625° in longitude, and a temporal resolution of 6 hr. The vertical resolution varies, but the pressure resolution is finer than 22 hPa for altitudes less than 10 km above mean sea level. MERRA-2 considers emissions of dust, sea salt, sulfate, and black carbon. Zamora et al. (2022) showed that MERRA-2 represents well dust and combustion aerosols in the Arctic. Biological particles can be important in the Arctic, especially in processes of sea ice melting and leads (Creamean et al., 2020) but they are unfortunately not available in MERRA-2 (see Text S3 in Supporting Information S1 for details on MERRA-2). The same analysis has been repeated considering Copernicus Atmospheric Monitoring System reanalysis (Inness et al., 2019) for mixing ratio of aerosols and similar results were obtained (not shown).

Surface type can play an important role in cloud properties: the presence of sea ice or open ocean influence the turbulent and heat fluxes which can impact cloud properties (Young et al., 2016). We categorized clouds according to two different underlying surface types: sea ice and open ocean using the National Snow and Ice Data Center (NSIDC) data set (Cavalieri et al., 2014) that identifies sea ice cover (Markus & Cavalieri, 2000; Markus et al., 2009). The algorithm provides sea ice concentration percentage with a spatial resolution of 12.5 km × 12.5 km poleward of 30° latitude (see Text S4 in Supporting Information S1 for details on the NSIDC data set).

The analysis is focused over the Arctic region, defined as latitudes poleward of 65°N, and the Southern Ocean from 2007 to 2010. The definition of the Southern Ocean may differ between studies, here we delimit the region with latitudes between 40°S and 60°S (see Table S1 in Supporting Information S1 for a summary of the different data sets).

3. Method

3.1. Quantifying the Thermodynamic Phase Distribution of Clouds

We have defined a cloud object as connected cloudy pixels surrounded by clear sky, and we categorize this cloud object as mixed phase if it contains at least one ice and one liquid pixel. Figure 1 shows schematic diagrams of the

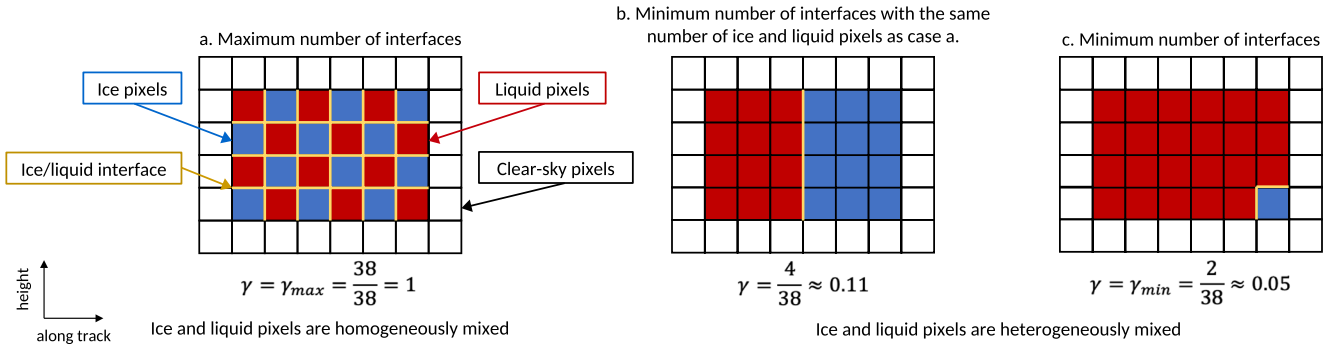

Figure 1. Schematic diagrams illustrating the vertical profiles of three theoretical extreme cases of the spatial distribution of cloud thermodynamic phase in mixed-phase clouds observed by an active space-based sensor. The presented cases represent a mixed-phase cloud where liquid and ice are maximally homogeneously mixed (a), a mixed-phase cloud where liquid and ice are maximally heterogeneously mixed (b), and a mixed-phase cloud with the minimum possible number of interfaces between the two phases (c). The associated γ parameter (cf. Equation 1) is displayed for each case.

vertical profiles of three different possible spatial configurations of mixed-phase clouds defined by the coexistence of ice and liquid pixels surrounded by clear-sky pixels. Figure 1a shows an idealized homogeneously mixed mixed-phase cloud. This cloud is comprised of a strict alternation between ice and liquid pixels that maximizes the liquid-ice interface that would theoretically result in a maximally efficient WBF process. Figure 1b shows an idealized maximally heterogeneously mixed mixed-phase cloud with the same number of ice and liquid pixels as in Figure 1a but organized such that the liquid-ice interface is relatively minimized. Finally, Figure 1c shows a mixed-phase cloud with the absolute minimum liquid-ice interface considering the same total number of pixels that would result in a minimally efficient WBF process.

To quantify the spatial homogeneity and surface area of the liquid-ice interface within mixed-phase clouds, we develop a metric, γ, defined as:

$$\gamma = \frac{N_{liq-ice}}{\max(N_{liq-ice})} \quad (1)$$

where $N_{liq-ice}$ is the number of liquid-ice interfaces within mixed-phase clouds and $\max(N_{liq-ice})$ is the maximum possible number of liquid-ice interfaces (see Text S5 in Supporting Information S1). Thus, for the homogeneous mixed-phase cloud in Figure 1a $\gamma = 1$, in Figure 1b $\gamma = 0.11$, and in Figure 1c $\gamma = 0.05$. Since we aim to ultimately improve the representation of mixed-phase clouds in GCMs, γ is retrieved for each cloud object, but averaged over a one-degree grid cell, to match the typical horizontal resolution of GCMs. We retrieved the γ parameter considering all the interfaces of liquid and ice in mixed-phase clouds and then we divide by the number of mixed-phase clouds within the grid cell to consider the average γ for each cloud. Most $1° \times 1°$ grid cells contain only one cloud. The spatial collocation of ERA-5 and MERRA2 has been done by averaging the data within the considered $1° \times 1°$ degree grid. For the temporal collocation, we considered the closest data from ERA5 and MERRA-2 to the DARDAR measurements within the $1° \times 1°$ grid.

3.2. Understanding the Controlling Factors of the Thermodynamic Phase Distribution

Atmospheric parameters are correlated with each other. The analysis of the impact of one parameter on a process without considering the intercorrelation between the different components is a common problem in Earth science, especially working with observations (Coopman, Garrett, et al., 2018; Gryspeerdt et al., 2016). For example, the impact of temperature on cloud thermodynamic phase cannot be directly quantified and assessed by examining the correlation between only cloud phase and temperature. In the present study, we consider a multilinear regression to study the impact of the atmospheric parameters on cloud thermodynamic phase homogeneity (Dobson & Barnett, 2018). This method aims to quantify the relative importance of meteorological parameters on γ.

Here, we perform a multilinear regression fit using several meteorological variables to predict the outcome, γ as follows:

$$\gamma_i = \beta_0 + \beta_1 x_{i,1} + \beta_2 x_{i,2} + \cdots + \beta_n x_{i,n} + \epsilon \quad (2)$$

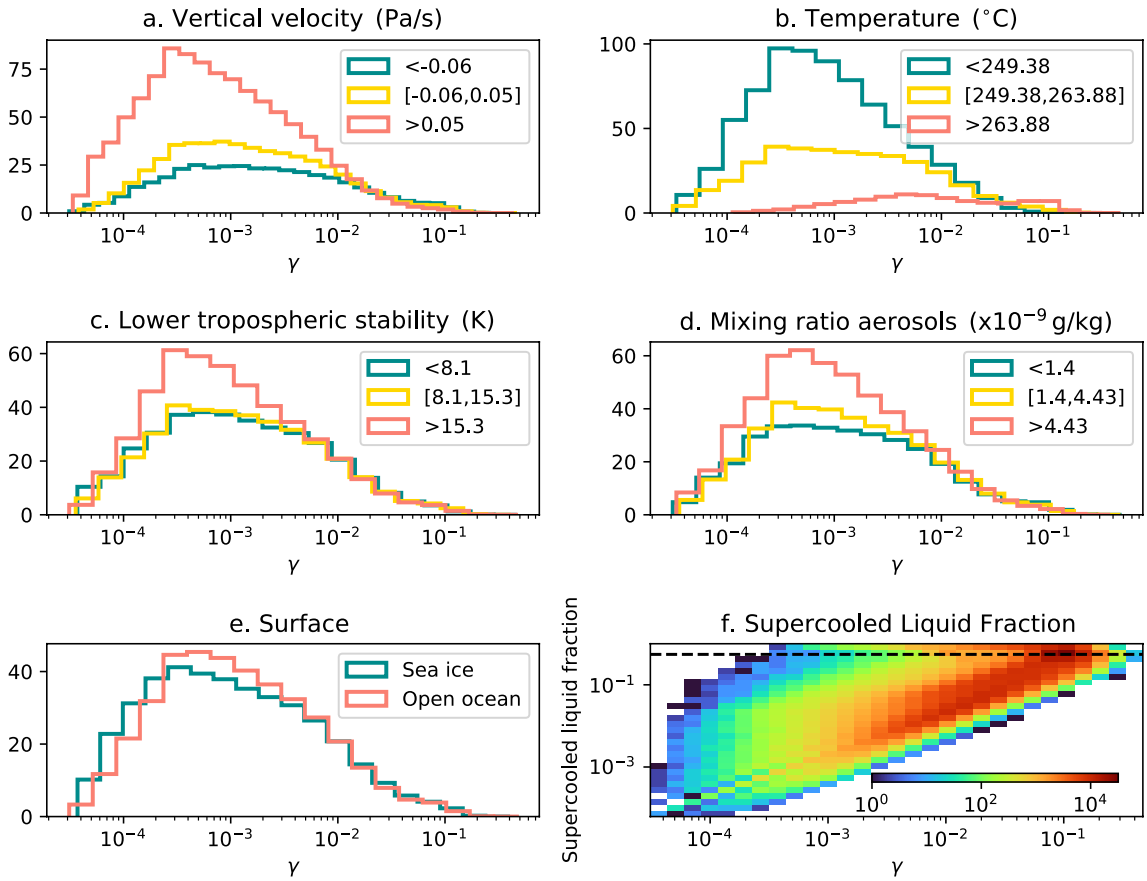

Figure 2. Distribution of γ for different regimes of vertical velocity for ascent regime only (a), temperature (b), LTS (c), mixing ratio of aerosols (d), and different type of surface—over sea ice and open ocean (e)—over the Arctic. The different regimes for subplots (a)–(d) are defined by values below the first quartile, above the third quartile and between the first and third quartiles. Kolmogorov-Smirnov tests performed on each parameter showed that the distributions are different, with a p-value of less than 0.05. The 2D histogram (f) represents the distribution of the supercooled liquid fraction and γ and the dashed line for supercooled liquid fraction equal to 0.6 is displayed.

where γ_i is the homogeneity parameter for the grid cell i, $x_{i,j}$ is the variable j associated to the grid cell, β_j is the slope coefficient associated to the parameter j, ϵ is the residual, and n is the total number of parameters. We do not consider parameters with a correlation coefficient greater than 0.2 to avoid including parameters that are correlated with each other (see Table S2 and Text S6 in Supporting Information S1).

We divide the data set in two: one data set trains the model (80% of the grid cells) and one data set tests the model (20% of the grid cells). The training and test data sets are used to evaluate the performance of the model applied to the data set and the capacity to predict γ as a function of meteorological conditions and aerosols via a r^2 value (see Text S7 in Supporting Information S1).

It is important to note that the present study does not focus on the impact of parameters on the occurrence of mixed phase clouds but rather the impact of the parameters on the spatial distributions of ice and liquid pixels.

4. Results

Figure 2 shows the normalized distribution of γ in the Arctic considering three regimes of vertical velocity (a), temperature (b), LTS (c), mixing ratio of aerosols (d), and considering grid cells associated with open ocean or sea ice (e). The unit of vertical velocity is Pa s^{-1}, so negative values are associated with updrafts and positive values with downdrafts. The regimes for the first four parameters are defined as grid cells for which the parameter is lower than the first quartile and higher than the third quartile. Our results show that γ is in general low, 90% of the data set has γ less than 0.11 (not shown): mixed phase clouds are most of the time not homogeneously mixed. We observe that high γ is associated with high updraft and temperature and low LTS and mixing ratio of aerosols.

For example, the median of γ is 0.010 for temperatures less than 249 K and is 0.074 for temperatures greater than 264 K. Surface type does not seem to play an important role on γ directly: the median of γ is equal to 0.024 when associated with both open ocean and sea ice. The results for the Southern Ocean are similar except that high γ is associated with high mixing ratio of aerosols (see Figure S1 in Supporting Information S1).

Figure 2f shows γ as a function of supercooled liquid fraction calculated in terms of frequency. The two parameters are positively correlated with each other for supercooled liquid fraction less than 0.6. This implies that the more liquid in mixed-phase clouds, the more homogeneously mixed the cloud is. However, when supercooled liquid fraction is greater than 0.6, γ decreases with increasing liquid cloud fraction. This can be explained by the fact that there are fewer isolated ice pixels. These results suggest that the spatial homogeneity of mixed-phase clouds is primarily controlled by the presence of liquid.

Many meteorological and aerosol parameters can impact cloud phase and it is difficult to disentangle the impact of one parameter on the cloud phase because they are intercorrelated with each other (Gryspeerdt et al., 2016). Statistical methods can help to infer the influence of one parameter considering the correlation with atmospheric parameters. Figure 3 shows the relative importance (β) of the 11 parameters in determining γ as quantified by the coefficients of the multilinear regression. First, we present the results for the Arctic region (Figures 3a–3d). The correlation coefficients r^2 between $\gamma^{predicted}$ and γ^{test} are rather low for the different regimes because the multiple linear regression considers only linear relations between γ and the variables from Equation 2, but most of the relations are nonlinear leading to low r^2. Nevertheless, our results are satisfactory at the first order, that is, considering linear relations between γ and the variables, with a r^2 between 0.17 and 0.3.

We observe that temperature is the parameter that best correlates with the cloud phase distribution over sea ice and open ocean in ascent and descent regions: for example, β associated with temperature is equal to 0.017 K^{-1}—3.8 times more important than the second most important parameter—over open ocean and ascent region. The higher the temperature, the more homogeneous the cloud phase is, in line with Figure 2. The mixing ratio of black carbon (BC) (MR_{BC}) is the second most important parameter that determines γ for every cloud surface and ascent/subsidence region with β between −0.001 and −0.003 kg g^{-1}. High M_{BC} is associated with a more heterogeneous cloud phase distribution. Results over ocean and sea ice show the same pattern. Moreover, in the subsidence regime, the vertical velocity is not important for determining γ as β is less than 0.002 s Pa^{-1} but it is important in the ascent regime as β is greater than 0.004 s Pa^{-1} for the different surface types.

Performing the same multilinear regression analysis over the Southern Ocean shows that the same conclusions drawn for the Arctic also apply to the Southern Ocean (Figures 3e and 3f): the parameter that contributes most to the spatial homogeneity of cloud thermodynamic phase is temperature. MR_{BC} is less important to determine γ but sea salt and Dimethylsulphide (DMS) influence more γ. The impact of vertical velocity is non-negligible in the ascent region unlike the subsidence regions.

A similar analysis examining the variation of γ as a function of a single parameter at a time (e.g., temperature) constraining for cloud regime defined by Moderate Resolution Imaging Spectroradiometer (MODIS) (Cho et al., 2021) revealed similar conclusions and support the robustness of these results (see Figure S2 and Text S8 in Supporting Information S1).

5. Discussion

First, the use of satellite data allows only the discussion of correlations between parameters, and we can only hypothesize about causes and consequences. Also, the various instrument limitations described in the data set section may bias γ, for example, small ice crystal might be undetected by the instruments or cloud bottom most layers cannot be detected due to the ground clutter. The relatively coarse spatial resolution of the data sets and especially MERRA-2 reanalysis may bias γ, the results, and the conclusions.

The low values of γ implies that liquid and ice pixels are arranged to minimize their interfaces in line with the representation of Arctic mixed-phase that typically consist of a layer of ice pixels below a layer of liquid pixels (de Boer et al., 2009). The spatial distribution of γ over the Arctic is fairly uniform (see Figure S3 and Text S9 in Supporting Information S1), except over Greenland which may be due to the detection of surface due to the uneven topography in this region (Blanchard et al., 2014). Over the Southern Ocean, we observe a slight east-west asymmetry of γ with slightly higher γ values over the Atlantic Arctic (see Figure S4 in Supporting Information S1) but it is not statistically significant.

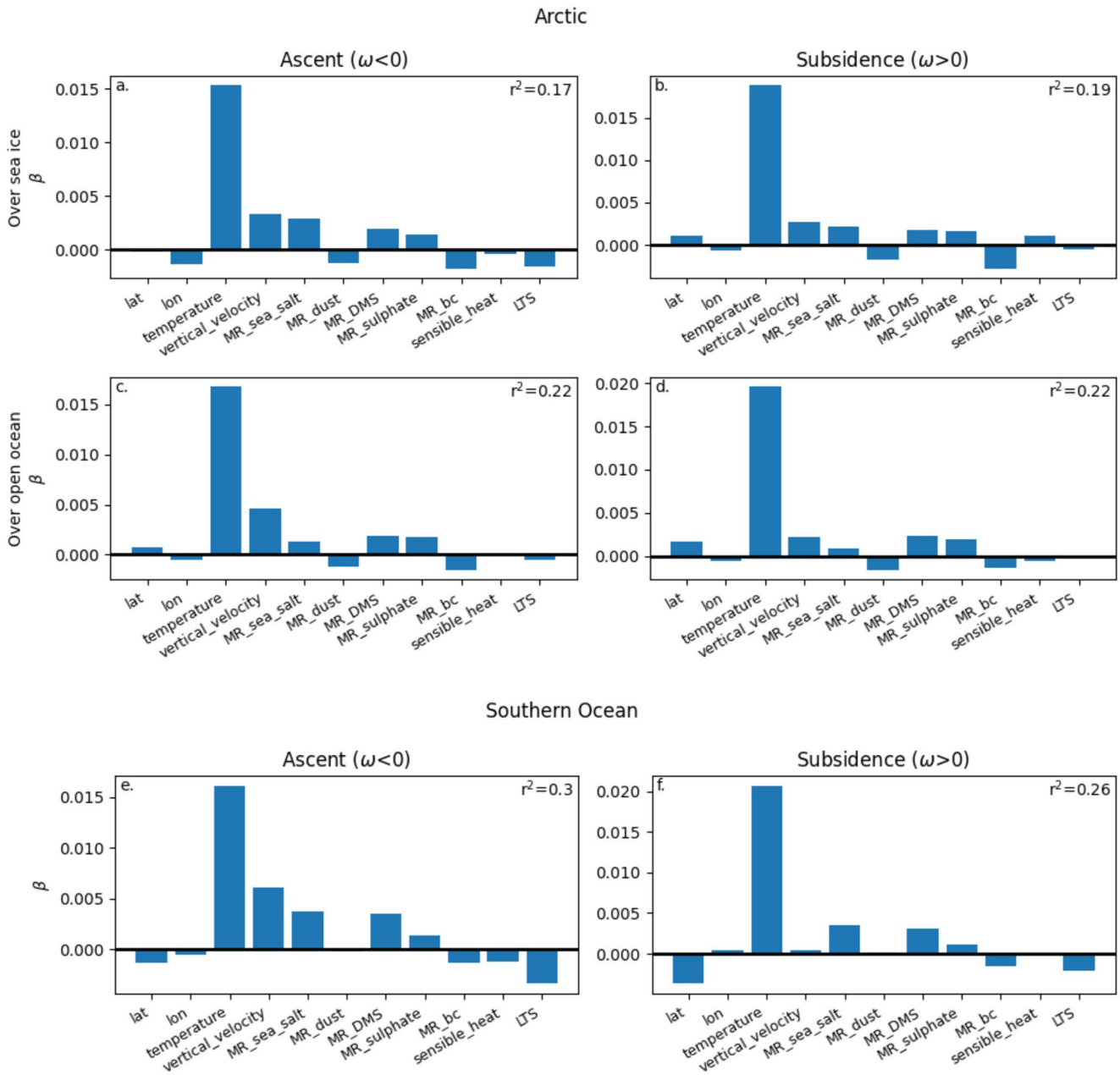

Figure 3. Parameters output from the multilinear regression fit for clouds over the Arctic (a–d) and Southern Ocean (e and f). We considered two regimes of vertical velocity (ω): ascent—vertical velocity less than 0 (a, c, and e)—and subsidence—vertical velocity greater than 0 (b, d, and f). We also considered two regimes of surface types over the Arctic: sea ice (a and b) and open ocean (c and d). Each regime has at least 15,000 grid cells to train the model. For each regime, the r^2 retrieved from $\gamma^{predicted}$ and γ^{test} is shown.

Since the results presented here are based on correlations it is therefore not possible to directly establish causality of the meteorological variables and their impact on physical processes. For example, radiative and dynamical processes that were not considered in this study may also influence the distribution of cloud hydrometeors (Morrison et al., 2011). Figure 2 shows that clouds with supercooled liquid fraction (SLF) are associated with low γ, so liquid pixels in predominantly ice clouds need to be arranged to minimize the liquid/ice interfaces: liquid pixels need to be clustered and arranged as large pockets. High SLF clouds are associated with high γ, ice pixels in mainly liquid clouds need to be arranged to maximize the liquid/ice interfaces: ice pixels need to be isolated and arranged as small pockets.

Figure 3 shows that cloud phase is more spatially homogeneously mixed at warmer temperatures. This result can be explained since temperature is the most important factor that determines the phase of clouds and the different

modes of nucleation (Knopf et al., 2018). The temperature dependence is directly related to the correlation between γ and the SLF shown in Figure 2f. The increase of γ with temperature could be explained by ice nucleation processes at high temperature: secondary ice processes (SIP) represent different ways to transition cloud phase from liquid to ice without INPs and for temperatures greater than homogeneous freezing and produce large concentrations of ice crystals at temperatures greater than −10°C (Field et al., 2017; Korolev & Leisner, 2020). Warmer air could also hold more water vapor and potentially larger cloud fractions after condensation, which could have an impact on γ, but the effect would be limited if the number of liquid-ice interfaces also increases.

The vertical velocity has an impact on the spatial distribution of the cloud thermodynamic phase in ascent regions. In the subsidence regime, dry air from above evaporates liquid droplets and ice crystals (Korolev et al., 2017), leading to the dissipation of the clouds. In low ascent regions, ice crystals grow at the expense of cloud droplets within mixed-phase clouds through the WBF process, rapidly glaciating the cloud (decreasing γ). In high ascent regions, moisture supplied from lower altitudes offsets the WBF process (Korolev et al., 2017). Therefore, strong updrafts maintain the coexistence of ice and liquid pockets within mixed-phase clouds and thus high values of γ. Arctic clouds tend to evolve when the atmosphere is stable (Klein & Hartmann, 1993) and form via clear-sky radiative cooling (Simpfendoerfer et al., 2019) but the atmosphere can become unstable in regions of strong ascent. We hypothesize that the impact of updraft on γ becomes less important, leading to a positive correlation between γ and vertical velocity and reveals the non-linearity between the two parameters (see Figure S5 in Supporting Information S1).

The thermodynamic phase of mixed-phase clouds associated with high mixing ratios of sulfate and DMS are heterogeneously mixed. We speculate that sulfate and DMS aerosols can act as CCN which can impact glaciation processes. Droplet fragmentation during freezing can happen if the surface of droplets freezes before its interior and the difference in pressure conducts frozen droplets to explode in multiple ice crystals (Korolev & Leisner, 2020). This process is more efficient when cloud droplets are larger (Rangno & Hobbs, 2001; Rosenfeld et al., 2011). Similarly to the WBF process, SIP is potentially more efficient when the phase is heterogeneously mixed. SIP processes decrease γ and the phase transition would be more important if γ is initially high (homogeneously mixed) than if γ is initially low (heterogeneously mixed). Therefore, ice and liquid pixels can co-exist over a longer period of time, thus increasing γ. In addition, sulfate coating on INP can inhibit ice nucleation (Archuleta et al., 2005; Grenier et al., 2009) resulting in fewer but larger ice crystals that are susceptible to precipitation at the expense of nonprecipitating clouds (Blanchet & Girard, 1994). Therefore, large crystal precipitation may mitigate and balance the WBF process and would be associated with a higher γ.

BC aerosols can act as efficient INPs (Bond et al., 2013; Gorbunov et al., 2001) and can have a strong impact on increasing the cloud glaciation temperature (Lohmann & Feichter, 2001). The role of BC in cloud glaciation remains uncertain due to its complexity (Bond et al., 2013; Hoose & Möhler, 2012; Kanji et al., 2017, 2020; Vergara-Temprado et al., 2018) but our results suggest that it is important for the spatial distribution of liquid and ice within a cloud. For the different surface types and the different updrafts, we observe that the mixing ratio of BC is negatively correlated with γ. We hypothesize that if the concentration of BC increases and if it acts as an efficient INP, the glaciation temperature increases too, so liquid pockets, which tend to be large and occur frequently within mixed-phase clouds, would glaciate, therefore decreasing γ. On the other hand, BC can also act as a CCN (Maskey et al., 2017) decreasing the glaciation temperature. Therefore, BC can have a competing effect depending on whether it is an efficient INP or CCN but our results suggest that the INP effect of BC dominates as mentioned by Coopman, Riedi, et al. (2018) for aerosols from combustion sources.

γ is the lowest in summer for the Arctic and in fall in the Southern Ocean while not statistically relevant due to the associated uncertainties (see Text S10 and Figure S6 in Supporting Information S1). We constrained the multilinear regression analysis for each season (not shown), and the βs were similar to Figure 3. Therefore, the spatial distribution of the cloud phase changes between seasons but the factors most correlated with the heterogeneity parameter are the same.

Finally, while this study focuses on the spatial distribution of liquid and ice hydrometeors within mixed-phase clouds and the meteorological parameters that contribute to it, it is notable that cloud microphysical properties also exert a significant impact. In particular, Coopman et al. (2021) showed that liquid cloud droplet effective radius at cloud-top is correlated with cloud ice fraction but does not impact the density of ice pockets within mixed-phase clouds.

6. Conclusions

Ice crystals and liquid cloud droplets are homogeneously mixed in numerical models, but observations show that the hydrometeors are clustered in ice and liquid pockets. The former assumption in GCMs has a strong impact on cloud processes and leads to a higher ice cloud fraction in GCMs than in the observations. The present study quantified the homogeneity of ice and liquid pockets within mixed-phase clouds using active spaced-based instruments. We also analyzed the relative importance of different meteorological parameters from reanalysis to predict the homogeneity of cloud phase using a multilinear regression fit.

From DARDAR observations, which are based on active measurements of clouds from a lidar and radar, we defined a new parameter to describe the spatial distribution of liquid and ice within mixed-phase clouds. This parameter quantifies the homogeneity of cloud phase: it determines if the ice and liquid pixels are homogeneously or heterogeneously mixed. We collocated cloud observations with reanalysis from MERRA-2 and ERA-5 to infer information from meteorological parameters and atmospheric aerosol content over the Southern Ocean and the Arctic region. A multilinear regression quantifies the relative importance of the parameters which describe the thermodynamic phase distribution within mixed-phase clouds constraining for surface type (sea ice and open ocean) and updraft and downdraft regimes. In the present analysis, we do not observe differences between surface types (open ocean and sea ice) and it might be due to the fact that we consider clouds decoupled from the surface.

Our analysis suggests that ice pockets are small and isolated within mixed-phase clouds whereas liquid pockets are large. The results show that temperature is the most important parameter for predicting the cloud phase distribution: higher temperatures are associated with more homogeneously mixed mixed-phase clouds. The second most important parameter is the mixing ratio of BC. The importance of the parameters differs for some regimes: sensible heat has a more important impact on the phase distribution over open ocean than sea ice and the vertical velocity is more important over the ascent region. The results can be applied to refine the representation of clouds in GCMs via improved parametrizations of the WBF process. This ultimately has implications for more accurate model simulations of climate and climate projections.

Acknowledgments
The authors sincerely acknowledge NSERC Grant RGPIN-2021-02920 and NASA Grant 80NSSC18K1599 for support. The authors sincerely thank three anonymous reviewers for constructive comments and useful suggestions that improved the quality of the manuscript. The authors also sincerely thank Dave Winker for valuable advice on the usage of the CALIPSO data set and Julien Delanoe for providing helpful guidance on the DARDAR data set in considering the uncertainty in the gamma metric. I. T. is sincerely indebted to Michael Bradford, Hankui Chai, Fengzhi Wu and Louis Tan for various valuable insights on the manuscript. The authors would also like to express sincere thanks to Lauren Zamora, Adam Sokel and Alexei Korolev for thought-provoking suggestions and feedback on this work. The authors express sincere gratitude to Ambrish Mangeshwar Raghoonundun for providing above and beyond technical support for this research. The authors sincerely appreciate support in computing, visualization, storage hardware and software provided by the Digital Research Alliance of Canada (https://alliancecan.ca/en), Calcul Quebec and Canada Foundation for Innovation (CFI)'s John R. Evans Leaders Fund (JELF) to enable this research. The authors thank Ruijia Yang for some suggestions and for participation in discussions at the initial stages of this work.

Data Availability Statement

The DARDAR-MASK v2 products are publicly available on the AERIS/ICARE Data Center (https://www.icare.univ-lille.fr/archive) after registration (https://www.icare.univ-lille.fr/asd-content/registration/register/).

ERA-5 data can be downloaded from the Copernicus Climate Change Service Climate Data Store (Hersbach et al., 2023). MERRA-2 data are available at MDISC (Global Modeling and Assimilation Office (GMAO), 2015).

NSIDC data can be downloaded at Meier et al. (2018).

References

Archuleta, C. M., DeMott, P., & Kreidenweis, S. (2005). Ice nucleation by surrogates for atmospheric mineral dust and mineral dust/sulfate particles at cirrus temperatures. *Atmospheric Chemistry and Physics*, *5*(10), 2617–2634. https://doi.org/10.5194/acp-5-2617-2005

Avery, M., Winker, D., Heymsfield, A., Vaughan, M., Young, S., Hu, Y., & Trepte, C. (2012). Cloud ice water content retrieved from the CALIOP space-based lidar. *Geophysical Research Letters*, *39*(5), L05808. https://doi.org/10.1029/2011GL050545

Bergeron, T. (1935). *On the physics of cloud and precipitation, procès verbaux de la séance de vu*. GGI à Lisbonne 19S3.

Blanchard, Y., Pelon, J., Eloranta, E. W., Moran, K. P., Delanoë, J., & Sèze, G. (2014). A synergistic analysis of cloud cover and vertical distribution from a-train and ground-based sensors over the high Arctic station eureka from 2006 to 2010. *Journal of Applied Meteorology and Climatology*, *53*(11), 2553–2570. https://doi.org/10.1175/JAMC-D-14-0021.1

Blanchet, J.-P., & Girard, E. (1994). Arctic "greenhouse effect". *Nature*, *371*(6496), 383. https://doi.org/10.1038/371383a0

Bodas-Salcedo, A., Mulcahy, J. P., Andrews, T., Williams, K. D., Ringer, M. A., Field, P. R., & Elsaesser, G. S. (2019). Strong dependence of atmospheric feedbacks on mixed-phase microphysics and aerosol-cloud interactions in HadGEM3. *Journal of Advances in Modeling Earth Systems*, *11*(6), 1735–1758. https://doi.org/10.1029/2019MS001688

Bond, T. C., Doherty, S. J., Fahey, D. W., Forster, P. M., Berntsen, T., DeAngelo, B. J., et al. (2013). Bounding the role of black carbon in the climate system: A scientific assessment. *Journal of Geophysical Research: Atmospheres*, *118*(11), 5380–5552. https://doi.org/10.1002/jgrd.50171

Cavalieri, D., Markus, T., & Comiso, J. (2014). AMSR-E/aqua daily l3 12.5 km brightness temperature, sea ice concentration, and snow depth polar grids, version 3. (Technical Report). *NASA National Snow and Ice Data Center Distributed Active Archive Center*. AMSR-E/AE_SI12. 003.

Ceccaldi, M., Delanoë, J., Hogan, R., Pounder, N., Protat, A., & Pelon, J. (2013). From CloudSat-CALIPSO to EarthCare: Evolution of the DARDAR cloud classification and its comparison to airborne radar-lidar observations. *Journal of Geophysical Research: Atmospheres*, *118*(14), 7962–7981. https://doi.org/10.1002/jgrd.50579

Cesana, G., & Chepfer, H. (2013). Evaluation of the cloud thermodynamic phase in a climate model using CALIPSO-GOCCP. *Journal of Geophysical Research: Atmospheres*, *118*(14), 7922–7937. https://doi.org/10.1002/jgrd.50376

Cesana, G., Waliser, D. E., Jiang, X., & Li, J. L. (2015). Multimodel evaluation of cloud phase transition using satellite and reanalysis data. *Journal of Geophysical Research: Atmospheres*, *120*(15), 7871–7892. https://doi.org/10.1002/2014JD022932

Chan, M. A., & Comiso, J. C. (2013). Arctic cloud characteristics as derived from MODIS, CALIPSO, and CloudSat. *Journal of Climate*, *26*(10), 3285–3306. https://doi.org/10.1175/JCLI-D-12-00204.1

Cho, N., Tan, J., & Oreopoulos, L. (2021). Classifying planetary cloudiness with an updated set of MODIS cloud regimes. *Journal of Applied Meteorology and Climatology*. https://doi.org/10.1175/jamc-d-20-0247.1

Chylek, P., & Borel, C. (2004). Mixed phase cloud water/ice structure from high spatial resolution satellite data. *Geophysical Research Letters*, *31*(14), L14104. https://doi.org/10.1029/2004GL020428

Coopman, Q., Garrett, T. J., Finch, D. P., & Riedi, J. (2018). High sensitivity of Arctic liquid clouds to long-range anthropogenic aerosol transport. *Geophysical Research Letters*, *45*(1), 372–381. https://doi.org/10.1002/2017GL075795

Coopman, Q., Hoose, C., & Stengel, M. (2021). Analyzing the thermodynamic phase partitioning of mixed phase clouds over the southern ocean using passive satellite observations. *Geophysical Research Letters*, *48*(7), e2021GL093225. https://doi.org/10.1029/2021gl093225

Coopman, Q., Riedi, J., Finch, D. P., & Garrett, T. J. (2018). Evidence for changes in Arctic cloud phase due to long-range pollution transport. *Geophysical Research Letters*, *45*(19), 10709–10718. https://doi.org/10.1029/2018GL079873

Creamean, J. M., Hill, T. C., DeMott, P. J., Uetake, J., Kreidenweis, S., & Douglas, T. A. (2020). Thawing permafrost: An overlooked source of seeds for Arctic cloud formation. *Environmental Research Letters*, *15*(8), 084022. https://doi.org/10.1088/1748-9326/ab87d3

D'Alessandro, J. J., Diao, M., Wu, C., Liu, X., Jensen, J. B., & Stephens, B. B. (2019). Cloud phase and relative humidity distributions over the southern ocean in austral summer based on in situ observations and CAM5 simulations. *Journal of Climate*, *32*(10), 2781–2805. https://doi.org/10.1175/JCLI-D-18-0232.1

de Boer, G., Eloranta, E. W., & Shupe, M. D. (2009). Arctic mixed-phase stratiform cloud properties from multiple years of surface-based measurements at two high-latitude locations. *Journal of the Atmospheric Sciences*, *66*(9), 2874–2887. https://doi.org/10.1175/2009JAS3029.1

Delanoë, J., & Hogan, R. J. (2008). A variational scheme for retrieving ice cloud properties from combined radar, lidar, and infrared radiometer. *Journal of Geophysical Research*, *113*(D7), D07204. https://doi.org/10.1029/2007JD009000

Delanoë, J., & Hogan, R. J. (2010). Combined CloudSat-CALIPSO-MODIS retrievals of the properties of ice clouds. *Journal of Geophysical Research*, *115*(4), D00H29. https://doi.org/10.1029/2009JD012346

Dobson, A. J., & Barnett, A. G. (2018). *An introduction to generalized linear models*. Chapman and Hall/CRC.

Field, P. R., Lawson, R. P., Brown, P. R. A., Lloyd, G., Westbrook, C., Moisseev, D., et al. (2017). Chapter 7. Secondary Ice Production—Current state of the science and recommendations for the future. *Meteorological Monographs*, AMSMONOGRAPHS–D–16–0014.1. https://doi.org/10.1175/AMSMONOGRAPHS-D-16-0014.1

Findeisen, W. (1938). Kolloid-meteorologische vorgänge bei neiderschlags-bildung. *Meteorologische Zeitschrift*, *55*, 121–133.

Forster, P., Storelvmo, T., Armour, K., Collins, W., Dufresne, J.-L., Frame, D., et al. (2021). The Earth's energy budget, climate feedbacks, and climate sensitivity. In V. Masson-Delmotte, P. Zhai, A. Pirani, S. L. Connors, C. Péan, S. Berger, et al. (Eds.), *Climate change 2021: The physical science basis. contribution of working group I to the sixth assessment report of the intergovernmental panel on climate change (chapter 7)* (pp. 923–1054). Cambridge University Press. https://doi.org/10.1017/9781009157896.009

Frey, W. R., & Kay, J. E. (2018). The influence of extratropical cloud phase and amount feedbacks on climate sensitivity. *Climate Dynamics*, *50*(7), 3097–3116. https://doi.org/10.1007/s00382-017-3796-5

Gelaro, R., McCarty, W., Suárez, M. J., Todling, R., Molod, A., Takacs, L., et al. (2017). The modern-era retrospective analysis for research and applications, version 2 (MERRA-2). *Journal of Climate*, *30*(14), 5419–5454. https://doi.org/10.1175/JCLI-D-16-0758.1

Gettelman, A., Liu, X., Ghan, S. J., Morrison, H., Park, S., Conley, A., et al. (2010). Global simulations of ice nucleation and ice supersaturation with an improved cloud scheme in the community atmosphere model. *Journal of Geophysical Research*, *115*(D18), D18216. https://doi.org/10.1029/2009JD013797

Global Modeling and Assimilation Office (GMAO). (2015). MERRA-2 inst3_3d_aer_Nv: 3d,3-hourly, instantaneous, model-level, assimilation, aerosol mixing ratio V5.12.4 [Dataset]. Goddard Earth Sciences Data and Information Services Center (GES DISC). https://doi.org/10.5067/LTVB4GPCOTK2

Gorbunov, B., Baklanov, A., Kakutkina, N., Windsor, H., & Toumi, R. (2001). Ice nucleation on soot particles. *Journal of Aerosol Science*, *32*(2), 199–215. https://doi.org/10.1016/S0021-8502(00)00077-X

Graham, R. M., Hudson, S. R., & Maturilli, M. (2019). Improved performance of ERA5 in Arctic gateway relative to four global atmospheric reanalyzes. *Geophysical Research Letters*, *46*(11), 6138–6147. https://doi.org/10.1029/2019GL082781

Grenier, P., Blanchet, J., & Muñoz-Alpizar, R. (2009). Study of polar thin ice clouds and aerosols seen by CloudSat and CALIPSO during midwinter 2007. *Journal of Geophysical Research*, *114*(D9), D09201. https://doi.org/10.1029/2008JD010927

Gryspeerdt, E., Quaas, J., & Bellouin, N. (2016). Constraining the aerosol influence on cloud fraction. *Journal of Geophysical Research: Atmospheres*, *121*(7), 3566–3583. https://doi.org/10.1002/2015JD023744

Hagihara, Y., & Okamoto, H. (2013). Global cloud distribution revealed by combined use of CloudSat/CALIPSO: Comparison using CALIPSO versions 2 and 3 data. In *AIP conference proceedings* (Vol. 1531, pp. 456–459). https://doi.org/10.1063/1.4804805

Hersbach, H., Bell, B., Berrisford, P., Biavati, G., Horányi, A., Muñoz-Sabater, J., et al. (2023). ERA5 hourly data on pressure levels from 1940 to present [Dataset]. Copernicus Climate Change Service (C3S) Climate Data Store (CDS). https://doi.org/10.24381/cds.bd0915c6

Hersbach, H., Bell, B., Berrisford, P., Hirahara, S., Horányi, A., Muñoz-Sabater, J., et al. (2020). The ERA5 global reanalysis. *Quarterly Journal of the Royal Meteorological Society*, *146*(730), 1999–2049. https://doi.org/10.1002/qj.3803

Hoose, C., & Möhler, O. (2012). Heterogeneous ice nucleation on atmospheric aerosols: A review of results from laboratory experiments. *Atmospheric Chemistry and Physics*, *12*(20), 9817–9854. https://doi.org/10.5194/acp-12-9817-2012

Inness, A., Ades, M., Agustí-Panareda, A., Barré, J., Benedictow, A., Blechschmidt, A.-M., et al. (2019). The CAMS reanalysis of atmospheric composition. *Atmospheric Chemistry and Physics*, *19*(6), 3515–3556. https://doi.org/10.5194/acp-19-3515-2019

Kalesse, H., de Boer, G., Solomon, A., Oue, M., Ahlgrimm, M., Zhang, D., et al. (2016). Understanding rapid changes in phase partitioning between cloud liquid and ice in stratiform mixed-phase clouds: An Arctic case study. *Monthly Weather Review*, *144*(12), 4805–4826. https://doi.org/10.1175/MWR-D-16-0155.1

Kanji, Z. A., Ladino, L. A., Wex, H., Boose, Y., Burkert-Kohn, M., Cziczo, D. J., & Krämer, M. (2017). Overview of ice nucleating particles. *Meteorological Monographs*, *58*, 1–1.33. https://doi.org/10.1175/AMSMONOGRAPHS-D-16-0006.1

Kanji, Z. A., Welti, A., Corbin, J. C., & Mensah, A. A. (2020). Black carbon particles do not matter for immersion mode ice nucleation. *Geophysical Research Letters*, *47*(11), e2019GL086764. https://doi.org/10.1029/2019GL086764

Kay, J. E., & Gettelman, A. (2009). Cloud influence on and response to seasonal Arctic sea ice loss. *Journal of Geophysical Research*, *114*(D18), D18204. https://doi.org/10.1029/2009JD011773

Klein, S. A., & Hartmann, D. L. (1993). The seasonal cycle of low stratiform clouds. *Journal of Climate*, *6*(8), 1587–1606. https://doi.org/10.1175/1520-0442(1993)006⟨1587:TSCOLS⟩2.0.CO;2

Knopf, D. A., Alpert, P. A., & Wang, B. (2018). The role of organic aerosol in atmospheric ice nucleation: A review. *ACS Earth and Space Chemistry*, *2*(3), 168–202. https://doi.org/10.1021/acsearthspacechem.7b00120

Komurcu, M., Storelvmo, T., Tan, I., Lohmann, U., Yun, Y., Penner, J. E., et al. (2014). Intercomparison of the cloud water phase among global climate models. *Journal of Geophysical Research: Atmospheres*, *119*(6), 3372–3400. https://doi.org/10.1002/2013JD021119

Korolev, A. (2007). Limitations of the Wegener–Bergeron–Findeisen mechanism in the evolution of mixed-phase clouds. *Journal of the Atmospheric Sciences*, *64*(9), 3372–3375. https://doi.org/10.1175/JAS4035.1

Korolev, A., Isaac, G. A., Cober, S. G., Strapp, J. W., & Hallett, J. (2003). Observations of the microphysical structure of mixed-phase clouds. *Quarterly Journal of the Royal Meteorological Society*, *129*(587), 39–66. https://doi.org/10.1256/qj.01.204

Korolev, A., & Leisner, T. (2020). Review of experimental studies of secondary ice production. *Atmospheric Chemistry and Physics*, *20*(20), 11767–11797. https://doi.org/10.5194/acp-20-11767-2020

Korolev, A., McFarquhar, G., Field, P. R., Franklin, C., Lawson, P., Wang, Z., et al. (2017). Mixed-phase clouds: Progress and challenges. *Meteorological Monographs*, *58*, 5.1–5.50. https://doi.org/10.1175/AMSMONOGRAPHS-D-17-0001.1

Korolev, A., & Milbrandt, J. (2022). How are mixed-phase clouds mixed? *Geophysical Research Letters*, *49*(18), e2022GL099578. https://doi.org/10.1029/2022GL099578

Lewis, J. R., Campbell, J. R., Stewart, S. A., Tan, I., Welton, E. J., & Lolli, S. (2020). Determining cloud thermodynamic phase from the polarized micro pulse lidar. *Atmospheric Measurement Techniques*, *13*(12), 6901–6913. https://doi.org/10.5194/amt-13-6901-2020

Listowski, C., Delanoë, J., Kirchgaessner, A., Lachlan-Cope, T., & King, J. (2019). Antarctic clouds, supercooled liquid water and mixed phase, investigated with DARDAR: Geographical and seasonal variations. *Atmospheric Chemistry and Physics*, *19*(10), 6771–6808. https://doi.org/10.5194/acp-19-6771-2019

Listowski, C., Rojo, M., Claud, C., Delanoë, J., Rysman, J.-F., Cazenave, Q., & Noer, G. (2020). New insights into the vertical structure of clouds in polar lows, using radar-lidar satellite observations. *Geophysical Research Letters*, *47*(17), e2020GL088785. https://doi.org/10.1029/2020GL088785

Lohmann, U., & Feichter, J. (2001). Can the direct and semi-direct aerosol effect compete with the indirect effect on a global scale. *Geophysical Research Letters*, *28*(1), 159–161. https://doi.org/10.1029/2000GL012051

Markus, T., & Cavalieri, D. J. (2000). An enhancement of the NASA team sea ice algorithm. *IEEE Transactions on Geoscience and Remote Sensing*, *38*(3), 1387–1398. https://doi.org/10.1109/36.843033

Markus, T., Stroeve, J. C., & Miller, J. (2009). Recent changes in Arctic sea ice melt onset, freezeup, and melt season length. *Journal of Geophysical Research*, *114*(12), 1–14. https://doi.org/10.1029/2009JC005436

Maskey, S., Chong, K. Y., Seo, A., Park, M., Lee, K., Park, K., et al. (2017). Cloud condensation nuclei activation of internally mixed black carbon particles. *Aerosol and Air Quality Research*, *17*(4), 867–877. https://doi.org/10.4209/aaqr.2016.06.0229

Matus, A. V., & L'Ecuyer, T. S. (2017). The role of cloud phase in Earth's radiation budget. *Journal of Geophysical Research: Atmospheres*, *122*(5), 2559–2578. https://doi.org/10.1002/2016JD025951

Meier, W. N., Markus, T., & Comiso, J. C. (2018). AMSR-E/AMSR2 unified L3 daily 12.5 km brightness temperatures, sea ice concentration, motion and snow depth polar grids, version 1 [Dataset]. NASA National Snow and Ice Data Center Distributed Active Archive Center. https://doi.org/10.5067/RA1MIJOYPK3P

Mioche, G., Jourdan, O., Ceccaldi, M., & Delanoë, J. (2015). Variability of mixed-phase clouds in the Arctic with a focus on the Svalbard region: A study based on spaceborne active remote sensing. *Atmospheric Chemistry and Physics*, *15*(5), 2445–2461. https://doi.org/10.5194/acp-15-2445-2015

Mitchell, J. F. B., Senior, C. A., & Ingram, W. J. (1989). CO_2 and climate: A missing feedback? *Nature*, *341*(6238), 132–134. https://doi.org/10.1038/341132a0

Morrison, H., de Boer, G., Feingold, G., Harrington, J., Shupe, M. D., & Sulia, K. (2011). Resilience of persistent Arctic mixed-phase clouds. *Nature Geoscience*, *5*(1), 11–17. https://doi.org/10.1038/ngeo1332

Nomokonova, T., Ebell, K., Löhnert, U., Maturilli, M., Ritter, C., & O'Connor, E. (2019). Statistics on clouds and their relation to thermodynamic conditions at ny-ålesund using ground-based sensor synergy. *Atmospheric Chemistry and Physics*, *19*(6), 4105–4126. https://doi.org/10.5194/acp-19-4105-2019

Peterson, C. A., Yue, Q., Kahn, B. H., Fetzer, E., & Huang, X. (2020). Evaluation of airs cloud phase classification over the Arctic Ocean against combined CloudSat–CALIPSO observations. *Journal of Applied Meteorology and Climatology*, *59*(8), 1277–1294. https://doi.org/10.1175/JAMC-D-20-0016.1

Pruppacher, H., & Klett, J. (2010). *Microphysics of clouds and precipitation* (Vol. 18). Springer Netherlands. https://doi.org/10.1007/978-0-306-48100-0

Rangno, A. L., & Hobbs, P. V. (2001). Ice particles in stratiform clouds in the Arctic and possible mechanisms for the production of high ice concentrations. *Journal of Geophysical Research*, *106*(D14), 15065–15075. https://doi.org/10.1029/2000JD900286

Rosenfeld, D., Yu, X., Liu, G., Xu, X., Zhu, Y., Yue, Z., et al. (2011). Glaciation temperatures of convective clouds ingesting desert dust, air pollution and smoke from forest fires. *Geophysical Research Letters*, *38*(21), L21804. https://doi.org/10.1029/2011GL049423

Shupe, M. D. (2007). A ground-based multisensor cloud phase classifier. *Geophysical Research Letters*, *34*(22), L22809. https://doi.org/10.1029/2007GL031008

Shupe, M. D. (2011). Clouds at Arctic atmospheric observatories. Part II: Thermodynamic phase characteristics. *Journal of Applied Meteorology and Climatology*, *50*(3), 645–661. https://doi.org/10.1175/2010JAMC2468.1

Shupe, M. D., Matrosov, S. Y., & Uttal, T. (2006). Arctic mixed-phase cloud properties derived from surface-based sensors at Sheba. *Journal of the Atmospheric Sciences*, *63*(2), 697–711. https://doi.org/10.1029/2001JD001106

Simpfendoerfer, L. F., Verlinde, J., Harrington, J. Y., Shupe, M. D., Chen, Y.-S., Clothiaux, E. E., & Golaz, J.-C. (2019). Formation of Arctic stratocumuli through atmospheric radiative cooling. *Journal of Geophysical Research: Atmospheres*, *124*(16), 9644–9664. https://doi.org/10.1029/2018JD030189

Solomon, A., de Boer, G., Creamean, J. M., McComiskey, A., Shupe, M. D., Maahn, M., & Cox, C. (2018). The relative impact of cloud condensation nuclei and ice nucleating particle concentrations on phase partitioning in Arctic mixed-phase stratocumulus clouds. *Atmospheric Chemistry and Physics*, *18*(23), 17047–17059. https://doi.org/10.5194/acp-18-17047-2018

Stephens, G. L., Vane, D. G., Boain, R. J., Mace, G. G., Sassen, K., Wang, Z., et al. (2002). The CloudSat mission and the A-Train: A new dimension of space-based observations of clouds and precipitation. *Bulletin of the American Meteorological Society*, *83*(12), 1771–1790. https://doi.org/10.1175/BAMS-83-12-1771

Tan, I., Storelvmo, T., & Zelinka, M. D. (2016). Observational constraints on mixed-phase clouds imply higher climate sensitivity. *Science*, *352*(6282), 224–227. https://doi.org/10.1126/science.aad5300

Tansey, E., Marchand, R., Protat, A., Alexander, S. P., & Ding, S. (2022). Southern ocean precipitation characteristics observed from CloudSat and ground instrumentation during the Macquarie Island Cloud and Radiation Experiment (MICRE): April 2016 to march 2017. *Journal of Geophysical Research: Atmospheres*, *127*(5), e2021JD035370. https://doi.org/10.1029/2021JD035370

Thompson, D. R., Kahn, B. H., Green, R. O., Chien, S. A., Middleton, E. M., & Tran, D. Q. (2018). Global spectroscopic survey of cloud thermodynamic phase at high spatial resolution, 2005–2015. *Atmospheric Measurement Techniques*, *11*(2), 1019–1030. https://doi.org/10.5194/amt-11-1019-2018

Vergara-Temprado, J., Holden, M. A., Orton, T. R., O'Sullivan, D., Umo, N. S., Browse, J., et al. (2018). Is black carbon an unimportant ice-nucleating particle in mixed-phase clouds? *Journal of Geophysical Research: Atmospheres*, *123*(8), 4273–4283. https://doi.org/10.1002/2017JD027831

Vignesh, P. P., Jiang, J. H., Kishore, P., Su, H., Smay, T., Brighton, N., & Velicogna, I. (2020). Assessment of CMIP6 cloud fraction and comparison with satellite observations. *Earth and Space Science*, *7*(2), e2019EA000975. https://doi.org/10.1029/2019EA000975

Wang, Z., Vane, D., Stephens, G., & Reinke, D. (2003). *Level 2 combined radar and lidar cloud scenario classification product process description and interface control document*. (Technical Report No. 1.0). Pasadena: Jet Propulsion Laboratory. Retrieved from https://www.cloudsat.cira.colostate.edu/cloudsat-static/info/dl/2b-cldclass-lidar/2B-CLDCLASS-LIDAR_PDICD.P_R04.20120522.pdf

Wegener, A. (1911). *Thermodynamik der atmosphäre*. JA Barth.

Winker, D. M., Hunt, W. H., & McGill, M. J. (2007). Initial performance assessment of CALIOP. *Geophysical Research Letters*, *34*(19), L19803. https://doi.org/10.1029/2007gl030135

Winker, D. M., Vaughan, M. A., Omar, A., Hu, Y., Powell, K. A., Liu, Z., et al. (2009). Overview of the CALIPSO mission and CALIOP data processing algorithms. *Journal of Atmospheric and Oceanic Technology*, *26*(11), 2310–2323. https://doi.org/10.1175/2009JTECHA1281.1

Young, G., Jones, H. M., Choularton, T. W., Crosier, J., Bower, K. N., Gallagher, M. W., et al. (2016). Observed microphysical changes in Arctic mixed-phase clouds when transitioning from sea ice to open ocean. *Atmospheric Chemistry and Physics*, *16*(21), 13945–13967. https://doi.org/10.5194/acp-16-13945-2016

Zamora, L. M., Kahn, R. A., Evangeliou, N., Groot Zwaaftink, C. D., & Huebert, K. B. (2022). Comparisons between the distributions of dust and combustion aerosols in MERRA-2, FLEXPART and CALIPSO and implications for deposition freezing over wintertime Siberia. *Atmospheric Chemistry and Physics Discussions*, *22*(18), 1–25. https://doi.org/10.5194/acp-22-12269-2022

Zelinka, M. D., Myers, T. A., McCoy, D. T., Po-Chedley, S., Caldwell, P. M., Ceppi, P., et al. (2020). Causes of higher climate sensitivity in CMIP6 models. *Geophysical Research Letters*, *47*(1), 1–12. https://doi.org/10.1029/2019GL085782

Zhang, M., Liu, X., Diao, M., D'Alessandro, J. J., Wang, Y., Wu, C., et al. (2019). Impacts of representing heterogeneous distribution of cloud liquid and ice on phase partitioning of Arctic mixed-phase clouds with NCAR CAM5. *Journal of Geophysical Research: Atmospheres*, *124*(23), 13071–13090. https://doi.org/10.1029/2019JD030502

Zhang, Y., Xie, S., Lin, W., Klein, S. A., Zelinka, M., Ma, P.-L., et al. (2019). Evaluation of clouds in version 1 of the E3SM atmosphere model with satellite simulators. *Journal of Advances in Modeling Earth Systems*, *11*(5), 1253–1268. https://doi.org/10.1029/2018MS001562

Zhao, M., & Wang, Z. (2010). Comparison of Arctic clouds between European center for medium-range weather forecasts simulations and atmospheric radiation measurement climate research facility long-term observations at the north slope of Alaska barrow site. *Journal of Geophysical Research*, *115*(D23), D23202. https://doi.org/10.1029/2010JD014285